Study intra-4f transitions of Sm^{3+} ions under direct photoexcitation in TiO_2

Study intra-4f transitions of Sm^{3+} ions under direct photoexcitation in TiO_2

O M Chapura*, L V Mikhnev, E A Bondarenko, A A Skomorokhov, R A Goncharov and A A Tsagikyan

North-Caucasus Federal University, Pushkin Street 1, Stavropol 355009, Russian Federation

*Email: ChapurOL-7@mail.ru

Abstract. A systematic study of photoluminescence transitions of samarium ion (Sm^{3+}) incorporated in titanium dioxide (TiO_2) powder with anatase structure has been performed. Perceptible changes of luminescence under direct excitation as compared with indirect excitation of Sm^{3+} in titanium dioxide (TiO_2:Sm^{3+}) have been detected. Measurements of photoluminescence excitation spectra for all detected radiative transition of Sm^{3+} were accomplished. The values of asymmetry ratio were calculated for different excitation wavelengths. The dependence of luminescent intensity on Sm^{3+} doping concentration in TiO_2 host was studied under direct and indirect excitation. Thus, evidences of the existence of the several Sm^{3+} sites in anatase TiO_2 have been presented in this work.

1. Introduction

Titanium oxide (TiO_2) is a promising material for solar energy [1], optics [2] and photocatalysis [3] because of its relatively high chemical stability, high refractive index and unique photocatalytic properties. Due to the fact that titanium oxide is a semiconductor with a large band gap, especially in the form of anatase (the band gap is 3.2 eV), it is an also attractive host for activation by rare earth ions. The introduction of rare-earth ions in titanium oxide leads to a significant modification of its properties, which expands of its potential application. As shown in [4, 5], the introduction of rare-earth ions leads to an enhancement of the photocatalytic activity of titanium oxide. In addition, the potential of using rare-earth doped titanium oxide as material for anode in dye-sensitized solar cell [6] and gas sensors [7, 8] was previously demonstrated. The introduction of rare-earth ions into the crystal lattice of titanium oxide makes it possible to obtain efficient orange phosphors, which can be used in light-emitting diodes [9].

Due to the large energy gap between the metastable $^4G_{5/2}$ level and the nearest lower level $^6F_{11/2}$, the samarium ion (Sm^{3+}) exhibits strong photoluminescence in the visible region. Recently, special attention has been paid to the research of the radiation efficiency under direct excitation of Sm^{3+} in various host due to the development of highly efficient GaN laser diodes, which have the emission band overlapped with one of the absorption bands of the Sm^{3+} [10]. The luminescent properties of Sm^{3+} in titanium oxide (TiO_2:Sm^{3+}) have been previously reported in the works [11–16]. Special mention should be made that the works presented earlier are dedicated to the study of host-sensitized luminescence. Thus, to the best of our knowledge, there is a lack of the papers dealing with research of Sm^{3+} luminescence under direct activator excitation.

In this way, the purpose of this work is to study the luminescence parameters of $TiO_2:Sm^{3+}$ under direct photoexcitation of samarium ion.

2. Materials and methods

2.1. Synthesis of nanoparticles $TiO_2:Sm^{3+}$

$TiO_2:Sm^{3+}$ samples were obtained by sol-gel method based on hydrolysis and peptization of titanium tetraisopropylate in anhydrous alcohol [17]. The initial reagents for synthesis were titanium tetraisopropylate ($Ti(OC_3H_7)_4$), isopropyl alcohol (C_3H_7OH), concentrated nitric acid (HNO_3), distilled water (H_2O), samarium oxide (Sm_2O_3). Reagent grade chemicals and distilled water with 18.2 MΩ·cm resistivity were used.

Initially, Sm_2O_3 was dissolved in hot nitric acid to form nitrate solution, which then evaporated until drying-out. Then the dry samarium nitrate was used for preparation of 0.05 M alcoholic solution. At the next stage of the synthesis $TiO_2:Sm^{3+}$, an alcoholic solution of titanium tetraisopropylate were prepared under constant magnetic stirring. Next, an alcoholic solution of samarium nitrate and distilled water was successively added dropwise to the titanium tetraisopropylate solution. After turbidity of the solution, nitric acid was added to it. The amount of titanium tetraisopropylate was selected so that its final concentration was 0.25 M. To study the dynamics of concentration quenching, samarium was taken in the range from 0.125 to 1.25 mol% compared to the concentration of titanium tetraisopropylate. Nitric acid and water were taken in relation to titanium tetraisopropylate as 2:1 and 4:1, respectively. The resulting sol was kept at room conditions for 48 hours until complete gelation.

The gel was dried at 100 °C for 24 hours. At the last stage, the sample was annealed for 2 h at a temperature of 700 ° C in oxidation atmosphere. The annealing was carried out using a laboratory electric furnace SNOL 7.2 / 1100.

2.2. Characterization methods

The structural properties of the obtained particles were studied by X-ray diffraction using the PANalytical Empyrean diffractometer. The diffraction patterns were collected using Cu Kα irradiation source (λ_{ex}=0.15406 nm). The method of scanning electron microscopy (SEM) was used to characterize the morphology of the synthesized samples. SEM images were obtained on a TESCAN MIRA3 microscope.

The photoluminescence, photoluminescence excitation and diffuse reflection spectra were measured on an automated installation assembled on the basis of a MDR-41 and MDR-23U monochromators (Lomo JSC). All spectral measurements were performed at room temperature. A high-pressure Xenon lamp was used as a source of excitation radiation in photoluminescence spectra measurement. The spectra of diffuse reflection and photoluminescence excitation were measured using a tungsten halogen lamp. The photoluminescence spectrum and photoexcitation of luminescence were corrected to instrumental response. MgO powder was used as a reference sample in all spectral measurements.

3. Results and discussion

3.1. Structural investigation of $TiO_2:Sm^{3+}$

Figure 1 shows of typical XRD pattern and SEM image of titanium dioxide particles doped Sm^{3+} and obtained via the sol-gel method. Figure 1(b) shows, that $TiO_2:Sm^{3+}$ powder is a mixture of agglomerated nanoparticles with the size below 100 nm.

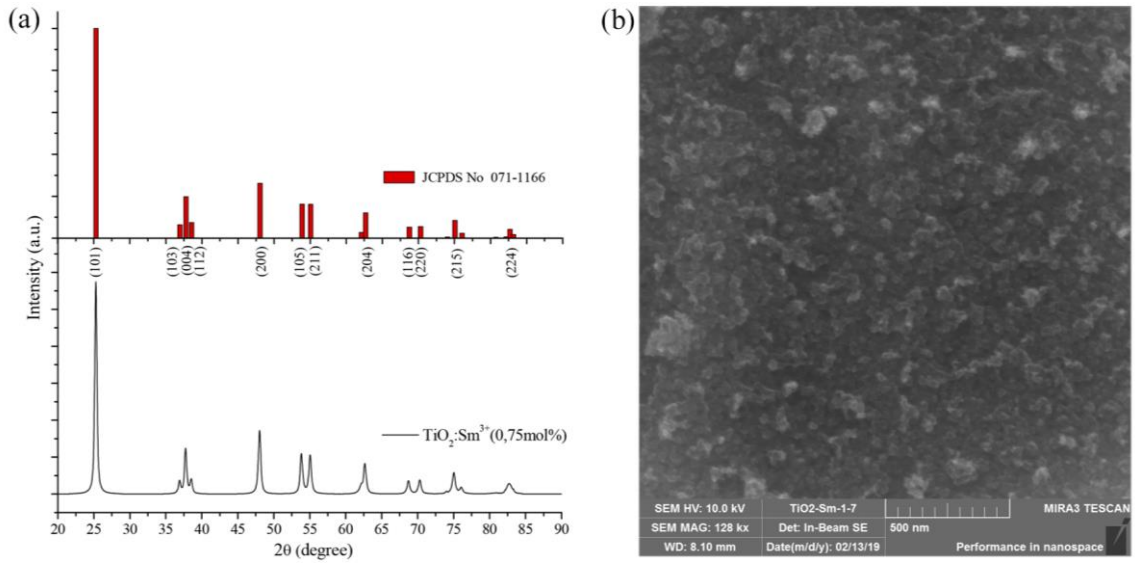

Figure 1. XRD pattern TiO_2:Sm^{3+} 0.75 mol% nanocrystalline powder and the standard card (JCPDS No 071-1166) for anatase TiO_2 (a) and an electron microscopic image of TiO_2:Sm^{3+} 0.75 mol% (b).

An analysis of the XRD patterns of the experimental samples showed the presence of the anatase phase of titanium dioxide (JCPDS No 071-1166). No trace of any others impurity phases such as samarium oxide were detected. The crystallite sizes calculated using the Debye-Scherrer formula decrease from 41.5 nm to 18.6 nm for samples contained 0.125 mol% and 1.25 mol% Sm^{3+} respectively. The results of measuring crystallite sizes for all experimental samples are presented in Table 1. This dependence of crystallite sizes is typical for titanium oxide particles doped with rare-earth ions [18].

Table 1. Crystallite size in dependence with Sm^{3+} concentration

Sm^{3+} concentration, mol%	Crystallite sizes, nm
0.125	41.5
0.25	36.4
0.5	27.6
0.125	23.5
0.25	21.2
0.5	18.6

3.2. Optical properties of TiO_2:Sm^{3+}

The estimation of the band gap for TiO_2:Sm^{3+} was carried out on the basis of the Tauc plot for direct semiconductors presented in Figure 2(a). In the present measurements, the Kubelka–Munk function has been used as a measure of absorption of TiO_2:Sm^{3+} samples.

The optical band gap of all TiO_2:Sm^{3+} samples were found to be around 3.2 eV [19]. In context with the crystallite sizes of experimental samples, that is much bigger than exciton Bohr radius of TiO_2 [20], we can make conclusion that the effect of quantum confinement on the band gap of our examples can be neglected.

Along with the fundamental absorption region, an activator absorption band with a maximum of 2.53 eV (488 nm) was also detected on the spectrum, shown in the inset of Figure 1, a. This relatively wide band can be correlated with the transition of the Sm^{3+} ion from the $^6H_{5/2}$ state to $^4I_{11/2}$+$^4I_{13/2}$ states. The presence of activator bands in the region of 411 nm was also shown previously in the work [21]. We associated this absorption band with the $^6H_{5/2}\rightarrow{}^6P_{3/2}$+$^6P_{5/2}$ transition.

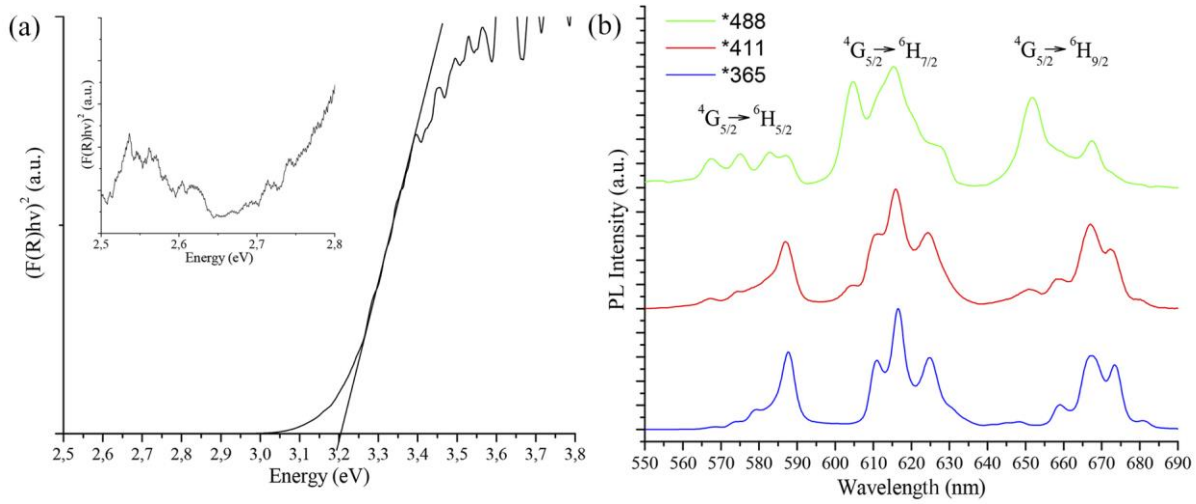

Figure 2. Tauc plot for nanoparticles of TiO_2:Sm^{3+}(0.75mol%) sample (a) and emission spectra of TiO_2:Sm^{3+}(0.75mol%) under direct (λ_{ex}=411 and 488 nm) and indirect (365 nm) excitation of Sm^{3+}.

Figure 2(b) shows the emission spectra obtained by excitation into activator absorption bands (411 and 488 nm) and fundamental absorption band (365 nm). As can be seen from Figure 2(b) emission spectrum obtained by indirect photoexcitation into consists of three groups of sharp spectral lines with the main maxima at 589, 616 and 667 nm. The intraconfigurational 4f-4f transitions of the Sm^{3+} from excited level $^4G_{5/2}$to stark splitting levels $^6H_{5/2}$, $^6H_{7/2}$ and $^6H_{9/2}$ well correspond to these maxima. However, in the case of direct excitation, one additional maximum appear to each of the multiplets from the shortwave side.

To reveal the nature of these additional peaks, the photoluminescence excitation spectra were measured for each of the observed spectral lines. The analysis of the resulting excitation spectra showed the presence of two types of photoexcitation spectral distributions, the shape of which is shown in Figure 3.

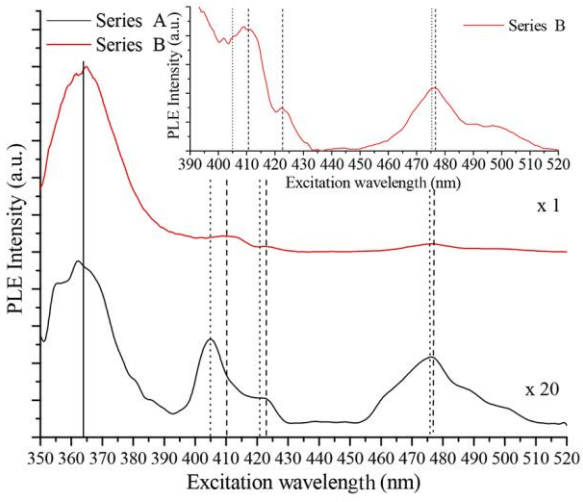

Figure 3. Photoluminescence excitation (PLE) spectrum for samarium series A and B in TiO_2:Sm^{3+}(0.75mol%) sample.

Therefore, it is possible to divide the emission lines into two series A and B with difference in the shape of the photoexcitation spectra. Series A consist of additional spectral lines (567, 604 and 648 nm), appearing under direct excitation. All spectral lines observed under indirect photoexcitation are included in series B.

Special mention should be made of the difference by the efficiency of activation of luminescence centers under excitation into the fundamental absorption band. Because, the lines of series A aren't observed in the photoluminescence spectra (Figure 2(b)) under excitation in fundamental absorption band, it can be concluded that the excitation efficiency of luminescence centers responsible for these transitions by indirect mechanism is small compared to the luminescence centers responsible for the spectral series B.

As can be seen from Figure 3, the excitation spectra of these two series have a different position of the bands in visible region. It should mention that the shape of the photoexcitation bands has a non-elementary character. Due to the fact that integrated intensity of band is produced by interplay of several transitions, the shift of the local maxima of the photoexcitation spectrum can be caused by the redistribution of the contributions of transitions Sm^{3+}. It should mention that probability of electric-dipole and magnetic-dipole transitions in different way depends from symmetry of luminescent center [22].

These differences indicate that, there are two sites of `Sm^{3+} in anatase TiO_2 with different photoluminescent characteristics. These luminescent centers were respectively named site A and site B.

To reveal the nature of the coordination environment of the luminescence center and its symmetry, the asymmetry ratio was determined upon different excitation wavelengths. Calculations of the asymmetry ratio have been performed to the procedure described in the work [23].However in the case of Sm^{3+}, asymmetry ratio is defined as integral intensity ratio of induced electric dipole transition $^4G_{5/2}\rightarrow{}^6H_{9/2}$ and magnetic-dipole transition $^4G_{5/2}\rightarrow{}^6H_{5/2}$ [10]. The analysis of the asymmetry ratio dependence, presented in Figure 4a, shows that the luminescent center responsible for additional spectral lines (site A) has value of the asymmetry ratio higher than the other luminescent center (site B). Thus, it can be concluded that Sm^{3+} placed in site A has lower symmetry than in site B.

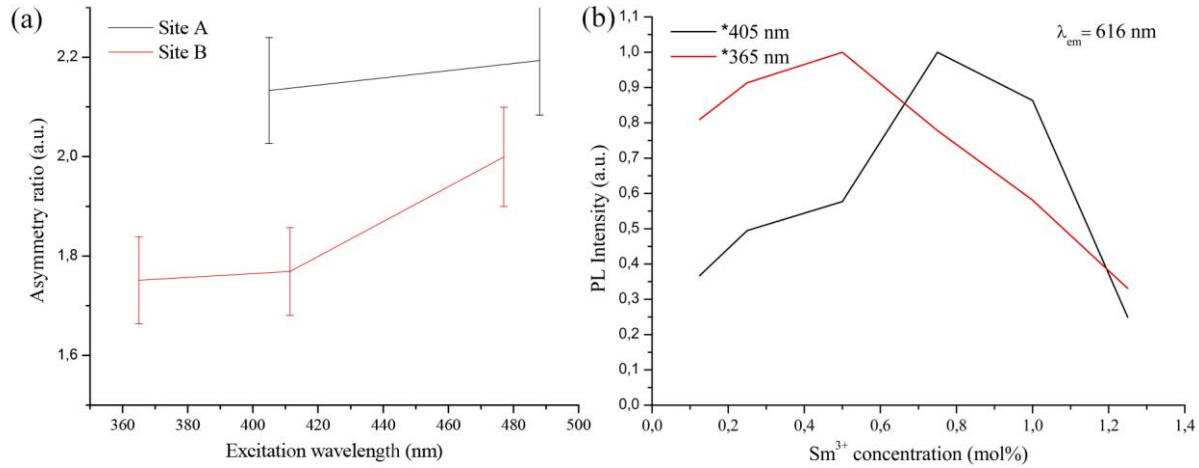

Figure 4. Asymmetrical ratio of TiO_2:Sm^{3+}(0.75mol%) as function of excitation wavelength (a) and normalized concentration dependences of $^4G_{5/2}\rightarrow{}^6H_{7/2}$ (λ_{em}=616 nm) intensity upon excitation wavelengths 365 and 405 nm (b).

Figure 4(b) shows normalized concentration dependences of the luminescence of the most intensive transition $^4G_{5/2}\rightarrow{}^6H_{7/2}$ (616 nm) under different excitation wavelengths 365 and 405 nm. As seen from figure 4(b) optimal concentration for Sm^{3+} shift depending on excitation wavelengths. So, optimum Sm^{3+} concentration for indirect excitation was determined 0.5 mol% whereas for direct Sm^{3+}

excitation (405 nm) is about 0.75 mol%. This difference can be explained by the existence of an additional energy transfer pathway, that inverse to the indirect mechanism of photoexcitation. Thus, there is probability transfer energy from Sm^{3+} to the TiO_2 host that can lead to energy dissipation.

4. Conclusion

The nanocrystalline TiO_2:Sm^{3+} with anatase structure was prepared by sol-gel methods. TiO_2:Sm^{3+}. The luminescence spectra of Sm^{3+} in TiO_2 host were obtained under direct and indirect photoexcitation. Additional spectral lines for each transition Sm^{3+} in visible region were observed upon direct excitation. The spectral distributions of luminescence photoexcitation for all detected spectral lines were measured. The symmetry of luminescent centres local surrounding was estimated using the asymmetry ratio. Photoluminescence intensity as a function of doping concentration has been studying under direct and indirect excitation. Numerous experimental evidences of two Sm^{3+} sites in the anatase crystal lattice were obtained.

References

[1] Roose B, Pathak S and Steiner U 2015 *Chem. Soc.Rev.***44** 8326–49
[2] Huang H, Xie Y, Zhang Z, Zhang F, Xu Q and Wu Z 2014 *Appl. Surf. Sci.* 2014 **293** 248–54
[3] Liu Y, Li Z, Green M, Just M, Li Y Y and Chen X 2017 *J. Phys. D: Appl. Phys.* **50(19)** 193003
[4] Reszczyńska J, Grzyb T, Wei Z, Klein M, Kowalsksa E, Ohtani B and Zaleska-Medynska A 2016 *Appl. Catal. B-Environ.* **181** 825–37
[5] Stengl V, Bakardjieva S and Murafa N 2009 *Mater. Chem. Phys.* **114(1)** 217–26
[6] Liu M, Hou Y and Qu X 2017 *J. of Mater. Res.* **32** 3469–76
[7] Eltermann M, Utt K, Lange S and Jaaniso R 2016 *Opt. Mater.* **51** 24–30
[8] Eltermann M, Kiisk V, Berholts A, Dolgov L, Lange S, Utt K and Jaaniso R 2018 *Sens. Actuators, B* 265 556–64
[9] Zhu C, Lv C, Gao Z, Wang C, Li D, Ma X and Yang D 2015 *Appl. Phys. Lett.* **107** 131103
[10] Lupei A, Tiseanu C, Gheorghe C, Voicu F 2012 *Appl. Phys. B* **108** 909–18
[11] Hu L, Song H, Pan G, Yan B, Qin R, Dai Q, Fan L and Li S and Bai X 2007 *J. Lumin.* **127** 371–6
[12] An G, Yang C, Zhou Y and Zhao X 2012 *Phys. Status Solidi A* **209(12)** 2583–8
[13] Vranjes M, Kuljanin-Jakovljević J, Ahrenkiel S P, Zekovića I, Mitrića M, Šaponjića Z and Nedeljkovića J M 2013 *J. Lumin.* **143** 453–8
[14] Chakraborty A, Debnath G H, Saha N R, Chattopadhyay D, Waldeck D H and Mukherjee P J. 2016 *Phys. Chem. C* **120**(**41**) 23870–82
[15] Chang M, Song Y, Chen J, Zhang X, Meng D, Zhua H , Shib Z, ZouaH and Shenga Y 2017 *J. Alloy Compd.* **725** 724–38
[16] Chang M, Zou H, Song Y, Chen J, Cui L, Sheng Y and Zheng K 2017 *J. Phys. Chem. Solids* **124** 100–10
[17] Mahshid S, Askari M and Ghamsari M S 2007 *J. Mater. Process. Technol.* **189** 296–300
[18] Setiawati E and KawanoK 2008 *J. Alloy Compd.* **451** 293–296
[19] Brik M G, Sildos I and Kiisk V 2010 *Physica B* **405** 2450–6
[20] Luca V 2009 *J. Phys. Chem. C* **113** 6367–80
[21] Kiisk V, Reedo V, Sild O and Sildos I 2009 *Opt. Mater.* **31** 1376–9
[22] K Binnemans 2015 *Coord. Chem. Rev.* **295** 1–45
[23] Kolesnikov I E, Povolotskiy A V, Mamonova D V, Kolesnikov E Y, Kurochkin A V, Lähderanta E and Mikhailov M D 2018 *J. Rare Earth* **36** 474–481